

Recent Results on Neutrino Oscillations

J. M. CONRAD

Nevis Laboratories, P.O. Box 137, Irvington, NY 10533, USA
E-mail: conrad@fnal.gov

This article reviews the many new results from neutrino oscillation searches which were presented at ICHEP '98. Exciting indications of neutrino oscillations have been seen in the solar neutrino deficit, atmospheric neutrino deficit and LSND excess. These indications and reported limits on oscillations are considered. Attempts to develop a theory which addresses all of the neutrino oscillation data are discussed. Some of the remaining questions and the future experiments which will help answer these questions are described.

This article reviews recent data on neutrino oscillations, focussing on the new results presented in Parallel Session 2 of the International Conference on High Energy Physics (ICHEP) '98. Section 1 provides an introduction to the formalism of neutrino oscillations and practicalities of understanding oscillation results. Section 2 reviews the present evidence for neutrino oscillations: the solar neutrino deficit, atmospheric neutrino deficit and LSND excess. Several recent experiments have completed extensive searches for oscillations and have established limits on oscillation parameters based on their null results. These are reviewed in section 3. Combining the positive indications and the limits permits construction of models for oscillations. Two types of models are considered in section 4. After considering all of the results, it is clear that the present data raise many questions. Some of the future experiments which may help resolve these questions are described in section 5.

1 Introduction to Neutrino Oscillations

The existence of neutrino oscillations would require a significant departure from the Standard Model. Oscillations imply that lepton flavor number is not conserved. Furthermore, at least one neutrino must be massive, which requires a right-handed partner to the neutrino. There are various ways to accommodate this extension to the Standard Model. For example, one can introduce iso-singlet partners ("sterile neutrinos").

At this point, if neutrinos are massive, we know that their mass is tiny. Kinematic distributions observed in weak decay can be used to place limits on the mass of outgoing neutrinos. This method has been used to obtain upper limits on the e , μ , and τ neutrinos from the decay channels listed in Tab. 1. It will be extremely difficult experimentally to measure m_{ν_μ} and m_{ν_τ} if these masses are at the level of, or smaller than, a few eV's. Further progress in the near future will have to come through searching for neutrino oscillations.

1.1 Neutrino Oscillation Formalism

If neutrinos have mass, it is likely that the mass eigenstates are different from the weak interaction eigenstates. In this case, the weak eigenstates can be written as mixtures of the mass eigenstates, for example:

$$\begin{aligned}\nu_e &= \cos\theta \nu_1 + \sin\theta \nu_2 \\ \nu_\mu &= -\sin\theta \nu_1 + \cos\theta \nu_2\end{aligned}$$

where θ is the "mixing angle." In this case, a pure flavor (weak) eigenstate born through a weak decay will oscillate into another flavor as the state propagates in space. This oscillation is due to the fact that each of the mass eigenstate components propagates with different frequencies if the masses are different, $\Delta m^2 = |m_2^2 - m_1^2| > 0$. In such a two-component model, the oscillation probability for $\nu_\mu \rightarrow \nu_e$ oscillations is then given by:

$$\text{Prob}(\nu_\mu \rightarrow \nu_e) = \sin^2 2\theta \sin^2 \left(\frac{1.27 \Delta m^2 (\text{eV}^2) L (\text{km})}{E (\text{GeV})} \right) \quad (1)$$

where L is the distance from the source, and E is the neutrino energy.

Most neutrino oscillation analyses consider only two-generation mixing scenarios, but the more general case includes oscillations between all three neutrino species. This can be expressed as:

$$\begin{pmatrix} \nu_e \\ \nu_\mu \\ \nu_\tau \end{pmatrix} = \begin{pmatrix} U_{e1} & U_{e2} & U_{e3} \\ U_{\mu1} & U_{\mu2} & U_{\mu3} \\ U_{\tau1} & U_{\tau2} & U_{\tau3} \end{pmatrix} \begin{pmatrix} \nu_1 \\ \nu_2 \\ \nu_3 \end{pmatrix}$$

This formalism is analogous to the quark sector, where strong and weak eigenstates are not identical and the resultant mixing is described conventionally by a unitary mixing matrix. The oscillation probability is then:

$$\begin{aligned}\text{Prob}(\nu_\alpha \rightarrow \nu_\beta) &= \delta_{\alpha\beta} - \\ &4 \sum_{j>i} U_{\alpha i} U_{\beta i} U_{\alpha j}^* U_{\beta j}^* \sin^2 \left(\frac{1.27 \Delta m_{ij}^2 L}{E} \right) \quad (2)\end{aligned}$$

Table 1: Direct neutrino mass measurements (see Ref. 1) from kinematic distributions of weak decays.

| Neutrino Type | Mass Limit | Process |
|---------------|----------------|---|
| Electron | $< \sim 10$ eV | ${}^3H \rightarrow {}^3He + e^- + \nu_e$ |
| Muon | < 170 keV | $\pi^+ \rightarrow \mu^+ + \nu_\mu$ |
| Tau | < 18.2 MeV | $\tau \rightarrow 5\pi(\pi^0) + \nu_\tau$ |

where $\Delta m_{ij}^2 = |m_i^2 - m_j^2|$. Note that there are three different Δm^2 (although only two are independent) and three different mixing angles.

Although in general there will be mixing among all three flavors of neutrinos, two-generation mixing is often assumed for simplicity. If the mass scales are quite different ($m_3 \gg m_2 \gg m_1$ for example), then the oscillation phenomena tend to decouple and the two-generation mixing model is a good approximation in limited regions. In this case, each transition can be described by a two-generation mixing equation. However, it is possible that experimental results interpreted within the two-generation mixing formalism may indicate very different Δm^2 scales with quite different apparent strengths for the same oscillation. This is because, as is evident from equation 2, multiple terms involving different mixing strengths and Δm^2 values contribute to the transition probability for $\nu_\alpha \rightarrow \nu_\beta$.

1.2 Neutrino Oscillation Experiments

From equation 1, one can see that three important issues confront the designer of the ideal neutrino experiment. First, if one is searching for oscillations in the very small Δm^2 region, then large L/E must be chosen in order to enhance the $\sin^2(1.27\Delta m^2 L/E)$ term. However if L/E is too large in comparison to Δm^2 , then oscillations occur rapidly. Because experiments have finite resolution on L and E , and a spread in beam energies, the $\sin^2(1.27\Delta m^2 L/E)$ averages to $1/2$ when $\Delta m^2 \gg L/E$ and one loses sensitivity to Δm^2 . Finally, because the probability is directly proportional to $\sin^2 2\theta$, if the mixing angle is small, then high statistics are required to observe an oscillation signal.

There are two types of oscillation searches: “disappearance” and “appearance.” To be simplistic, consider a pure source of neutrinos of type x . In a disappearance experiment, one looks for a deficit in the expected flux of ν_x . Appearance experiments search for $\nu_x \rightarrow \nu_y$ by directly observing interactions of neutrinos of type y . The case for oscillations is most persuasive if the deficit or excess has the (L/E) dependence predicted by the neutrino oscillation formula (equation 1).

Let us say that a hypothetical perfect neutrino oscillation experiment sees no oscillation signal, based on N

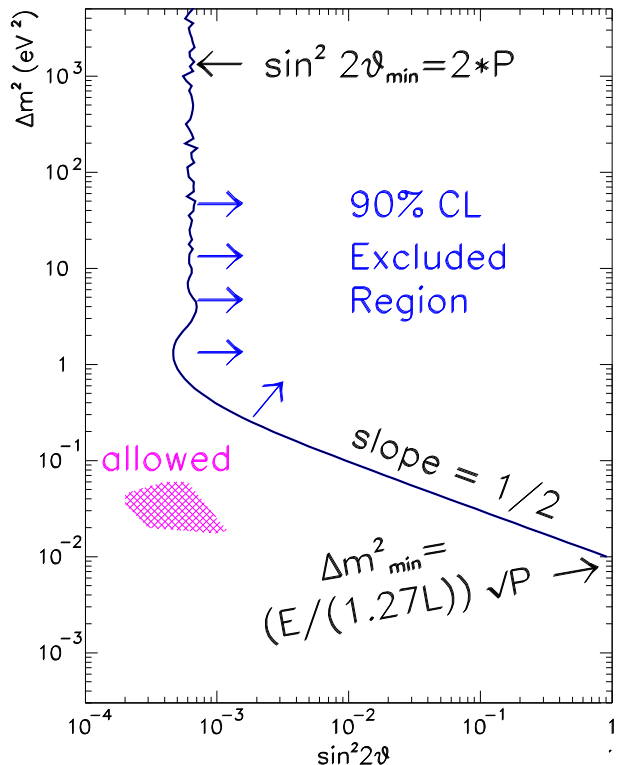


Figure 1: Generic example of a neutrino oscillation plot. The region to the right of the solid line is excluded at 90% CL. The shaded blob represents an “allowed” region.

events. The experimentors can rule out the probability for oscillations at some confidence level. A typical choice of confidence level is 90%, so in this case, the limiting probability is $P = 1.28\sqrt{N}/N$. There is only one measurement and there are two unknowns, so this translates to an excluded region within $\Delta m^2 - \sin^2 2\theta$ space. As shown in Fig. 1, this is indicated by a solid line, with the excluded region on the right. At high Δm^2 , the limit on $\sin^2 2\theta$ is driven by the experimental statistics. The L and E of the experiment drive the low Δm^2 limit.

The imperfections of a real experiment affect the limits which can be set. Systematic uncertainties in the efficiencies and backgrounds reduce the sensitivity of a given experiment. Background sources introduce multiple flavors of neutrinos in the beam. Misidentification of the interacting neutrino flavor in the detector can mimic oscillation signatures. In addition, systematic uncertainties in the relative acceptance versus distance and energy need to be understood and included in the analysis of the data. These systematics are included in the 90% CL excluded regions presented by the experiments in this paper.

The most convincing signature for oscillations is a statistically and systematically significant signal (as opposed to deficit) with dependence on L and E as predicted for oscillations. This has not yet been observed. Deficits have been observed in the expected rate of two neutrino sources: solar and atmospheric. A signal has been observed by the LSND experiment, but it is not at 5σ significance and the L and E dependence has not yet been clearly demonstrated.

Indications of neutrino oscillations appear as allowed regions, indicated by shaded areas (see example in Fig. 1), on plots of Δm^2 vs. $\sin^2 2\theta$.

1.3 Small Statistics Experiments with Background

Care must be taken when comparing excluded and allowed regions near the boundaries. First, one should remember that a 90% CL exclusion limit means that if a signal were in this region, 10% of the time it would not be seen. Second, there is no consensus within the physics community on the method for determining allowed regions and limits. Although in most cases, the deviations of the different methods are small, there are cases for which the disagreements are significant. As an example, consider Fig. 2, from Ref. 4. The details of the experimental results presented in this plot will be considered later. At this point, the reader should consider the shaded area to be an allowed region from an oscillation experiment (LSND) and the curves to represent the different statistical interpretations of 90% exclusion regions of the same set of experimental data (KARMEN 2).

In a hypothetical analysis, take μ to be the expected

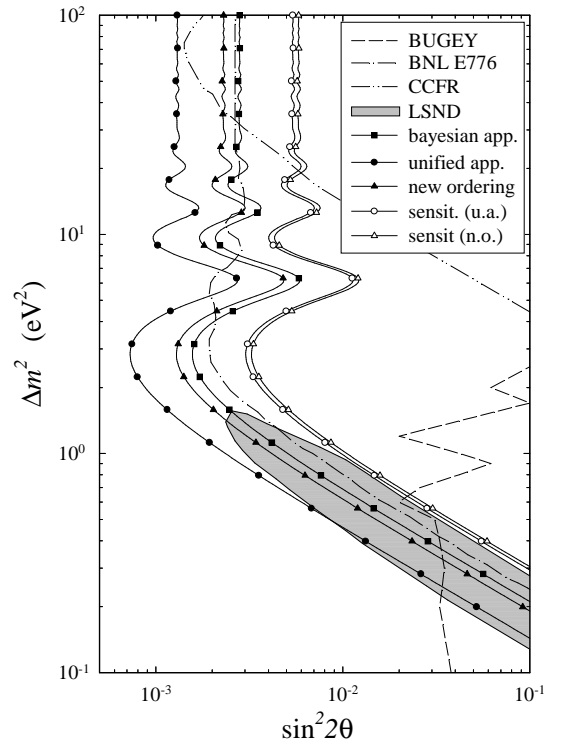


Figure 2: Range of possible interpretations of the KARMEN data. “Unified app” refers to the Feldman-Cousins Method, while “new ordering” refers to the Giunti Method. As per the Feldman-Cousins recommendation, the sensitivities associated with the analysis methods are also shown. (plot from Ref. 4)

signal and b to be the average expected background, and $n = \mu + b$ to be the total number of expected events. The experiment will observe some number of events, n_{obs} , which is not necessary equal to n . How is the measurement, n_{obs} , related to an estimate of μ , the true signal? In other words, what can n_{obs} tell us about the underlying physics?

In principle, the method is straightforward. We can construct two curves, $n_1(\mu, \alpha)$ and $n_2(\mu, \alpha)$ such that the probability for n to be between n_1 and n_2 is α . Typically, α is chosen to be 90%. For small statistics, a Poisson probability distribution is used. We then invert the relationship, obtaining the functions $\mu_1(n, \alpha)$ and $\mu_2(n, \alpha)$. Thus, n_{obs} implies that the signal, μ , lies somewhere between $\mu_1(n_{obs}, \alpha)$ and $\mu_2(n_{obs}, \alpha)$ with probability α . In practice, the construction of $n_1(\mu, \alpha)$ and $n_2(\mu, \alpha)$ can be done in various ways, and this forms the heart of this controversy.

The method which has been accepted in the past, and was previously endorsed by the Particle Data Group,² has an inherent inconsistency, as pointed out by Feldman and Cousins.³ In this method, n_1 is chosen such that $n < n_1(\mu, \alpha)$ with probability $(1 - \alpha)/2$ and n_2 is chosen such that $n > n_2(\mu, \alpha)$ with probability $(1 - \alpha)/2$. This gives you a central confidence interval based on a two sided Gaussian distribution in the case of a signal. But in the case of a limit, you have only a one sided confidence interval with $n < n_1(\mu, \alpha)$ with probability $(1 - \alpha)$. Thus your treatment of the data “flip-flops,” to use the terminology of Feldman-Cousins, depending on whether you are setting a limit or determining a signal region.

Feldman-Cousins developed a new method which is now adopted by the Particle Data Group, called “The Unified Approach.” In this approach, you order the n possibilities by the function $R(n) = \text{Prob}(n|\mu b)/\text{Prob}(n|\mu_{best}b)$ where $\mu_{best}(n) = \mu$ with maximum probability for n and b . The technique is to first order the $R(n)$ ’s from largest to smallest (thus the method is based on “likelihood ordering”), then sum the $R(n)$ values until you reach $\text{Prob} = \alpha$.

This Unified Approach has good features and drawbacks. By design, there is now a smooth transition between limits and signals – no more flip-flopping. But, if an experiment sees a number of events smaller than background, then this method sets a stringent upper bound on μ , *not because of sensitivity to small signals but because of the fact that too few background events are observed.*

Feldman-Cousins recognized this problem in their paper³ and raised the questions: “Why should an experiment claim credit for expected backgrounds when it is clear, in that particular experiment, there were none? Or why should a well-designed experiment which has no background and observes no events be forced to report a higher upper limit than a less well-designed experi-

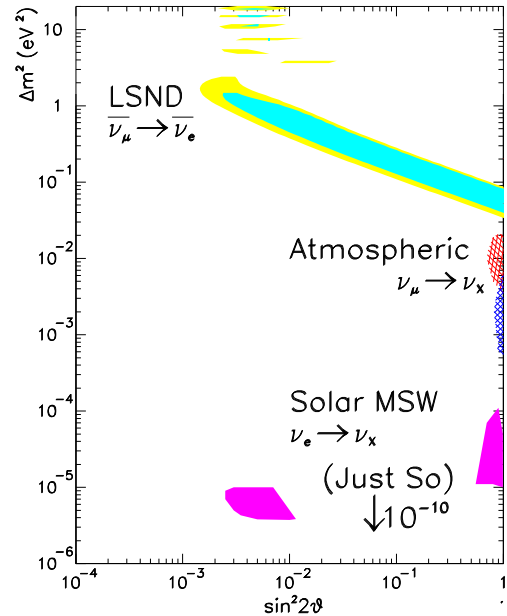


Figure 3: Hints for oscillations come from three sources: solar neutrinos, atmospheric neutrinos and accelerator produced neutrinos (LSND). The solar neutrino deficit has two possible oscillation solutions, MSW and Just-So (see text). Allowed regions for these three indications are presented here. Note that some regions are already addressed by exclusion experiments discussed in section 3.

ment which expects backgrounds, but, by chance, observes none?” The Feldman-Cousins prescription for this quandary is that an experiment which sees a low background fluctuation quote both the limit and the experimental sensitivity, where “sensitivity” is defined as the average expected limit if an experiment with no true signal, only background, were performed many times. This lets readers draw conclusions based their own personal opinion of what is acceptable.

In a recent paper,⁴ Giunti proposes a new method of ordering classical confidence intervals which guarantees a smooth transition from the limit to signal region while resulting in a weaker improvement in confidence level for the case where the background fluctuates low. In this case, $\mu_{best}(n)$ is replaced by $\mu_{ref}(n) = \int_0^\infty \mu P(\mu|n, b) d\mu$ where $P(\mu|n, b)$ is the Bayesian probability distribution for a constant $\mu \geq 0$. The data are then likelihood ordered according to $R(n) = \text{Prob}(n|\mu b)/\text{Prob}(n|\mu_{ref}b)$.

Comparison of the two methods demonstrates the relative stability of the limit with background fluctuations. Consider Fig. 2, which addresses an experiment in which 2.88 ± 0.013 background events are expected and zero events are observed. The two recent methods calculate very similar sensitivities of the experiment, as indicated by the open symbols. The Unified Approach (Feldman-Cousins) experimental sensitivity is 4.4 events while the New Ordering Approach (Giunti) sensitivity is 4.9 events. The limits are radically differ-

ent, however. The Unified Approach sets the limit as $\mu_{90\%CL} = 1.1$ events, which is better than the sensitivity by better than a factor of four. The New Ordering Approach sets a limit at 1.9 events. This is not far from the sensitivity.

A more conservative alternative is to use a Bayesian approach. Arguably, if less background is observed than expected, then one may be overestimating the background. Therefore one should set a limit assuming that $n_{obs} = b$, in this case, zero. Therefore this method sets the limit at 2.3 events, as shown on Fig. 2.

In summary, there is disagreement about how to handle data in the case of background plus a small expected signal. If an experiment sees the expected background, then the differences in the statistical methods are relatively small, but when the background fluctuates low there can be significant differences in limits. The reader should be skeptical of strong conclusions drawn in cases of small statistics. The goal now should be high statistics, low systematics experiments designed to address the hints for oscillations which have been observed.

2 Experiments Reporting Evidence for Oscillations

Three different sources of neutrinos have shown deviations from the expectation, consistent with oscillations. The first, called the ‘‘Solar Neutrino Deficit,’’ is a low rate of observed ν_e ’s from the sun. The data are consistent with $\Delta m^2 \sim 10^{-10} \text{eV}^2$ or $\Delta m^2 \sim 10^{-5} \text{eV}^2$, depending on the theoretical interpretation. The second, called the ‘‘Atmospheric Neutrino Deficit,’’ refers to neutrinos produced by decays of mesons from cosmic ray interactions in the atmosphere. An observed anomalously low ratio of ν_μ/ν_e can be interpreted as oscillations with $\Delta m^2 \sim 10^{-3} \text{eV}^2$. The third observation is an excess of $\bar{\nu}_e$ events in a $\bar{\nu}_\mu$ beam by the LSND experiment, with $\Delta m^2 \sim 10^{-1} \text{eV}^2$. Fig. 3 summarizes the allowed regions from these results. In this section each case is considered in detail.

2.1 The Solar Neutrino Deficit

As shown in Fig. 4, three different types of experiments have observed fewer neutrinos from the sun than expected from the Standard Solar Model (SSM).⁵ The first observation of this ν_e deficit was made using a Cl target in the Homestake mine by Davis and collaborators.⁶ Four additional experiments have confirmed these observations. The GALLEX and SAGE experiments search for electron neutrino interactions in a Ga target.⁷ The Kamiokande and Super Kamiokande (‘‘Super K’’) experiments observe $\nu_e + e \rightarrow \nu_e + e$ reactions in water.⁸ The gallium and water target experiments indicate a deficit

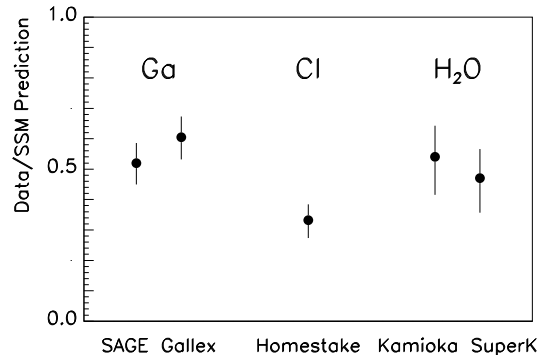


Figure 4: Ratio of measurements from five solar neutrino experiments, to the SSM (BP98) prediction.

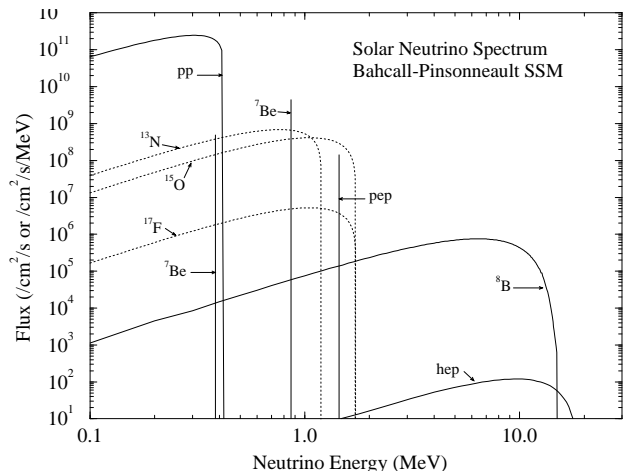


Figure 5: Neutrino fluxes as a function of energy from the sun as predicted in Ref. 13

of $\sim 1/2$, while the Cl experiment is lower. Results from GALLEX (D. Vignaud) and Super K (M. Vagins, M. Takita) are reported in these proceedings.

The solar data have been gathered over an extended period of time and many systematic checks on efficiencies and calibrations have been performed. For example, the Super K experiment has installed a LINAC at the detector for *in situ* calibration from 5 to 16 MeV. As a second example, the GALLEX experiment, which presented final results at this conference, doped their detector with ^{71}As , which decays to the signature ^{71}Ge . Recovery was measured to be $99.8 \pm 0.8\%$. This is one of many source tests performed by the GALLEX group and described at this conference.

Each type of solar experiment has a different energy threshold for observing ν_e interactions, and thus is sen-

Table 2: Fraction of ν_e 's expected from reactions in the Standard Solar Model for the three types of solar neutrino experiments.

| | Super K/ Kamioka | Homestake | GALLEX/SAGE |
|--------------------|---------------------|-----------|-------------|
| pp | | | 0.538 |
| ${}^7\text{Be}$ I | | | 0.009 |
| ${}^7\text{Be}$ II | | 0.150 | 0.264 |
| ${}^8\text{Be}$ | 1 | 0.775 | 0.105 |
| pep | | 0.025 | 0.024 |
| ${}^{13}\text{N}$ | | 0.013 | 0.023 |
| ${}^{15}\text{O}$ | | 0.038 | 0.037 |

sitive to different reactions producing neutrinos in the sun. The characteristic range of solar ν energies from each production mechanism is shown in Fig. 5. Major sources of solar neutrinos for each experiment are listed in Tab. 2. The “*hep*” (${}^3\text{He} + p \rightarrow {}^4\text{He} + e^+ + \nu_e$) process neutrino contribution is $\sim 10^{-4}$ of the ${}^8\text{B}$ contribution in most solar models, which is too low to be listed in Tab. 2, thus Super K sees effectively 100% ${}^8\text{B}$ neutrinos. Recently, however, it has been pointed out that the *hep* flux is not well constrained and could be twenty times larger than past models have predicted.⁹ With this increase, the *hep* neutrinos still remain a small component of the Super K flux, but the expected neutrino energy distribution changes slightly. The effect of this shift is discussed below.

Two important theoretical issues related to the solar neutrino fluxes are the fusion cross sections and the temperature of the solar interior. Consensus is developing on the systematic uncertainties associated with the dominant solar fusion cross sections. A recent comprehensive analysis¹⁰ of the available information on nuclear fusion cross sections important to solar processes provides the best values along with estimated uncertainties. These are included in the uncertainty in the SSM value for the ratio of data to prediction shown in Fig. 4. The flux of neutrinos from certain processes, particularly ${}^8\text{B}$, depends strongly upon temperature. Recent results in helioseismology have provided an important test of the SSM.¹¹ The sun is a resonant cavity, with oscillation frequencies dependent upon $U = P/\rho$, the ratio of pressure to density. Helioseismological data confirm the SSM prediction of U to better than 0.1%.¹² Helioseismological data are not included in the data used to determine the SSM, therefore this is an entirely independent cross-check of the model. The systematic error associated with temperature dependence is included in the theoretical error on the SSM prediction.

Interpreting the deficit of solar neutrinos as a signal for oscillations, one calculates the vacuum oscillation

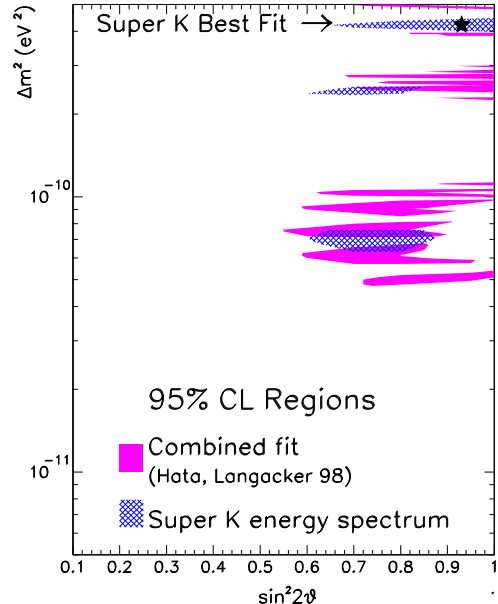


Figure 6: Allowed regions in the Δm^2 vs $\sin^2 2\theta$ parameter space from the four solar neutrino experiments assuming vacuum oscillations.

probability using equation 1, as shown in Fig. 6. Vacuum oscillations are often referred to as the “Just So Hypothesis” because this theory assumes that the position of the earth from the sun is at a distance which is an oscillation maximum. The energy of the neutrinos (only a few MeV) combined with the long path length from the sun to the earth ($\sim 10^{11}m$) results in allowed regions of Δm^2 which are very low ($\Delta m^2 \sim 10^{-10}eV^2$). In Fig. 6, an analysis of the overall fluxes¹³ is compared to the recent energy spectrum analysis from Super K, showing that the overlap of these two analyses is limited. Increasing the *hep* neutrino flux, as discussed above, modestly improves the agreement between overall flux and energy spectrum data.⁹

An alternative oscillation scenario, referred to as the MSW (Mikheyev-Smirnov-Wolfenstein) solution,¹⁴ includes “matter effects.” These effects occur because at low energies, the electron neutrino has both charged- and neutral-current elastic scattering with electrons, while the ν_μ and ν_τ experience only neutral-current scattering. The additional ν_e interactions introduce a phase shift as the mass state, which is a combination of flavor eigenstates, propagates. This leads to an increase in the oscillation probability:

$$\text{Prob}(\nu_e \rightarrow \nu_\mu) = (\sin^2 2\theta/W^2) \sin^2 (1.27W \Delta m^2 L/E) \quad (3)$$

where $W^2 = \sin^2 2\theta + (\sqrt{2}G_F N_e (2E/\Delta m^2) - \cos 2\theta)^2$ and N_e is the electron density. In a vacuum, where $N_e = 0$,

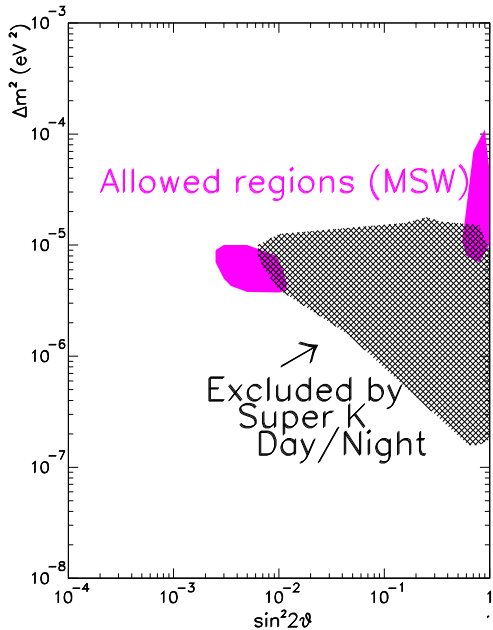


Figure 7: Solid: Allowed regions from the solar neutrino experiments, including the MSW effect. Hatched: Excluded (90% CL) region due to no day-night effect.

this reduces to equation 1. But within the sun, where the electron density varies rapidly, “MSW resonances,” or large enhancements of the oscillation probability can occur. It is also possible to have matter effects occur as neutrinos travel through the earth. For this reason, Super K has searched for a “day-night effect” – a difference in interaction rate at night due to the MSW effect in the earth’s core.

Results of a combined analysis of the solar neutrino data within the MSW framework are shown in Fig. 7. Allowed regions are indicated by the two solid areas, which are referred to as the small mixing angle (SMA) solution and large mixing angle (LMA) solution. Super K has seen no evidence of a day-night effect. As a result, a region indicated by the hatched area can be excluded at 90% CL. For more information, see the contribution by M. Vagins in these proceedings.

The recent data have been compared to the SSM in a global analysis by Bahcall, Krastev and Smirnov.¹⁵ The MSW SMA solution provided the best fit, with $\Delta m^2 = 5 \times 10^{-6} \text{eV}^2$ and $\sin^2 2\theta = 5.5 \times 10^{-3}$. The confidence level of the fit was 7%. The confidence level for the LMA solution was $\sim 1\%$. The Just-So solution gave a best

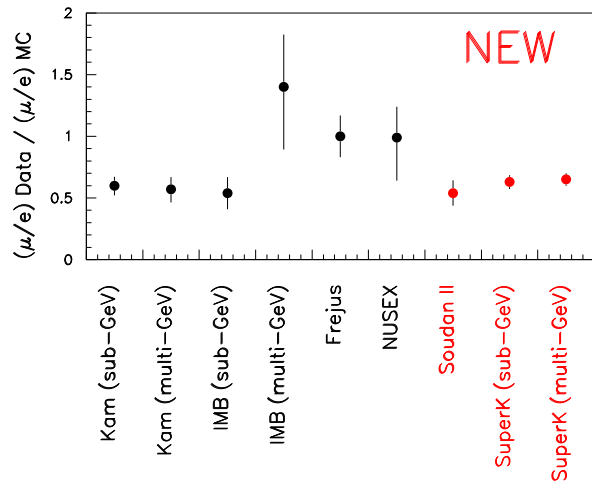


Figure 8: $(\nu_\mu/\nu_e)_{data}/(\nu_\mu/\nu_e)_{MC}$ for atmospheric experiments. The three newest results are listed at right.

fit of $\Delta m^2 = 6.5 \times 10^{-11} \text{eV}^2$ and $\sin^2 2\theta = 0.75$, with a 6% CL. Increasing the *hep* neutrino flux by a factor of 20 above the SSM improves the confidence level of all of these fits.⁹ The SMA solution increases to $\sim 20\%$, the LMA solution to $\sim 5\%$ and the “Just-So” to $\sim 15\%$. Although the confidence levels of the fits are relatively low, all three solutions are still possible.

The confidence level of fits which do not include oscillations is very low. The data are inconsistent with the SSM-without-oscillations at the 10σ level. If one allows the flux from each neutrino source to have an arbitrary normalization, fits can be obtained which are inconsistent at only the 3.5σ level, but are excluded by the helioseismology measurements. Therefore, oscillations appear to be the best explanation for the solar neutrino deficit.

2.2 The Atmospheric Neutrino Deficit

Neutrinos may be produced in the upper atmosphere. They result from cosmic rays colliding with atmospheric nucleons, producing mostly pions which then decay into muons and muon-neutrinos. The resulting muons may also decay, producing a muon- and an electron-flavored neutrino. Thus, this decay chain is expected to produce a two-to-one ratio for ν_μ to ν_e .

Atmospheric neutrinos have been detected through their charged-current interactions in detectors on the earth’s surface. The sensitivity of these detectors to electrons and muons varies over the observed energy range. For example, electron events are mostly contained in the detector, while muon events have longer range and escape the detector at higher energies. Therefore, the results are

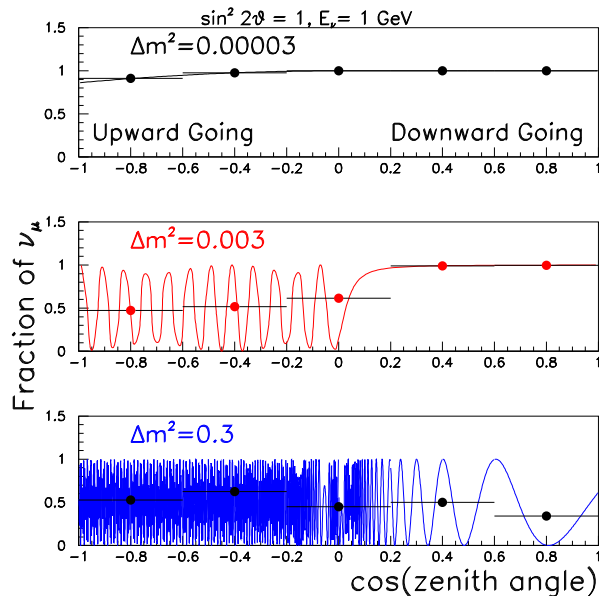


Figure 9: Disappearance of ν_μ due to oscillations as a function of cosine of zenith angle for three regions of Δm^2 . Resolution of the experiments and limitations of statistics smooth rapid oscillations such that the data will tend to look like the points

often divided into sub-GeV (contained) and multi-GeV (partially-contained) samples.

The observed ratio of muon to electron neutrino events divided by the ratio of events calculated in a Monte Carlo simulation ($R = (\nu_\mu/\nu_e)_{data}/(\nu_\mu/\nu_e)_{MC}$) for nine atmospheric neutrino analyses is reported in Fig. 8. The newest results are reported in these proceedings by H. Gallagher for Soudan and C. McGrew and M. Takita for Super K. Within statistics, all experiments are consistent with $R \sim 60\%$. This deviation from the expected ratio of one is called the “Atmospheric Neutrino Deficit.”

If the atmospheric neutrino deficit is due to neutrino oscillations, then one would expect a change in R as a function of neutrino path length. Neutrinos which are produced in interactions directly above the detector, called “downward-going,” traverse $L \sim 10\text{km}$. Neutrinos which are produced on the opposite side of the earth, called “upward-going,” travel $L \sim 10,000\text{km}$. Traditionally, the path of the neutrino is described by $\cos\theta_z$, where θ_z is the zenith angle measured from directly above the detector. It should be noted that the actual path length, L , is rapidly changing with $\cos\theta_z$. As an example, the R dependence *vs.* $\cos\theta_z$ for oscillations of 1 GeV ν_μ 's which are “disappearing” is shown in Fig. 9 for low, medium and high Δm^2 values. At very low Δm^2 , the probability

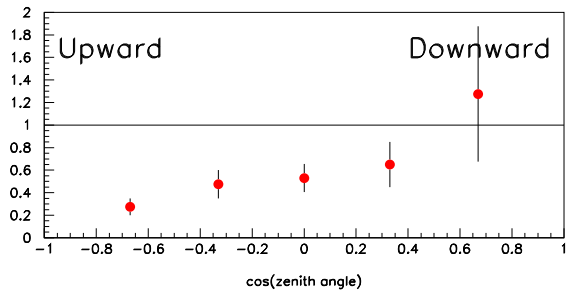


Figure 10: Zenith angle distribution of R from the Kamiokande experiment.

for oscillation is low, even for very long path lengths, so R will be consistent with one. At very high Δm^2 , even the neutrinos from above have had the opportunity to oscillate. The actual measurement will not resolve the rapid oscillations because of finite bin sizes, resolution of the detector, interaction physics and because the neutrinos produced in collisions in the atmosphere are not mono-energetic. The points on Fig. 9 are meant to indicate what might be measured for the three Δm^2 cases. A typical experiment would be unable to resolve rapid oscillations. This makes interpretation of the data, particularly in the moderate Δm^2 region, difficult.

In 1994, the Kamiokande group reported a zenith angle dependence of R .¹⁶ Comparing the Kamioka results shown in Fig. 10 to the expectations in Fig. 9, the data appear to be consistent with expectations for moderate Δm^2 . The best fit for $\nu_\mu \rightarrow \nu_\tau$ oscillations is $\Delta m^2 = 1.6 \times 10^{-2} \text{ eV}^2$.

The zenith angle dependence has been confirmed by recent data from Super K, as reported by C. McGrew, in these proceedings. The analysis is performed separately on sub-GeV ($p < 1.3 \text{ GeV}$) and multi-GeV ($p > 1.3 \text{ GeV}$) data samples. The sub-GeV are fully contained (FC) within the Super K detector while some the multi-GeV events are only partially contained (PC). Electron-like (ν_e scattering) candidates and muon-like (ν_μ scattering) candidates are presented as a function of $\cos\theta_z$ in Fig. 11 (points). The shaded region indicates the predicted flux of neutrinos without oscillations. There is a further $\sim 20\%$ normalization uncertainty associated with the flux which is reduced to $\sim 5\%$ when the ratio, R , is taken. The dashed line, which is labeled $\nu_\mu \rightarrow \nu_\tau$ for $\Delta m^2 = 0.0022\text{eV}^2$, shows that a good fit ($\chi^2/\text{DOF}=65.2/67$) is achievable with an oscillation hypothesis. Looking at the “e-like” data, one should note

Table 3: Δm^2 from $\cos \theta_z$ dependence of atmospheric neutrino experiments using the $\nu_\mu \rightarrow \nu_\tau$ oscillation hypothesis. Results that do not have a “best fit” quoted by the experiment are listed with the Δm^2 which is described as “consistent with” the data. Under “references,” listed names refer to contributions to these proceedings. All data but Kamiokande are preliminary.

| Experiment | Analysis | Δm^2 is ... | $\Delta m^2(\text{eV})^2$ | reference |
|------------|----------------|---------------------|---------------------------|----------------|
| Kamiokande | R | best fit | 1.6×10^{-2} | 18 |
| Kamiokande | up-going μ | best fit | 3.2×10^{-2} | 18 |
| Super K | R | best fit | 2.2×10^{-3} | McGrew, Takita |
| Super K | up-going μ | consistent with | 2.5×10^{-3} | McGrew, Takita |
| Soudan II | R | consistent with | $> 10^{-3}$ | Gallagher |
| MACRO | up-going ν | consistent with | 5×10^{-3} | Michael |
| MACRO | up-going μ | consistent with | 2.5×10^{-3} | Michael |

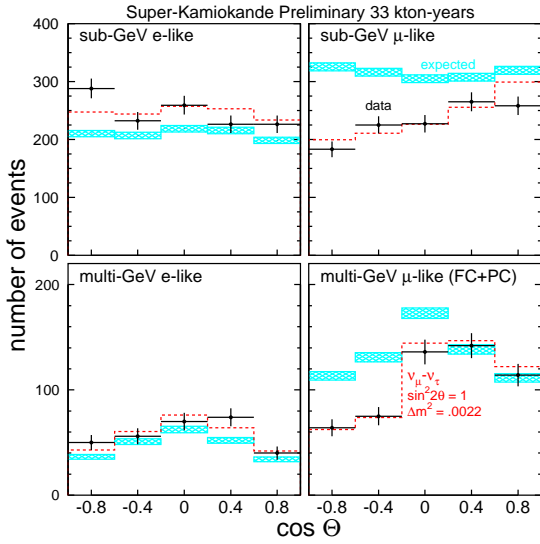


Figure 11: Rates of ν_e (“e-like”) and ν_μ (“ μ -like”) events at Super Kamiokande. The sub-GeV sample requires $p < 1.3$ GeV and the multi-GeV sample is $p > 1.3$ GeV. FC and PC refer to fully and partially contained events.

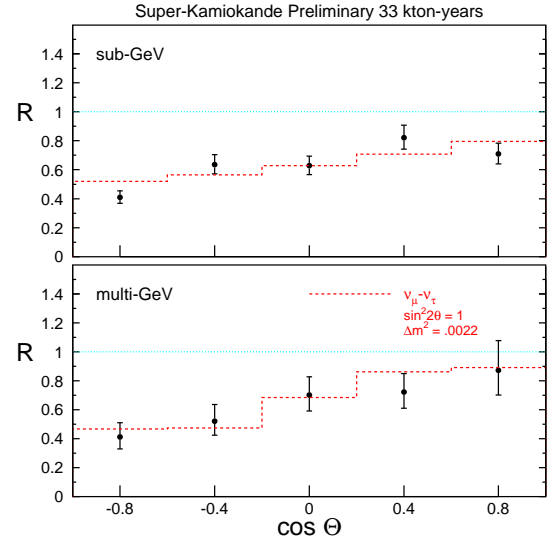


Figure 12: R for the Super Kamiokande experiment.

that there appears to be a small excess in the lowest $\cos \theta_z$ bin. Various authors have pointed out that this allows the Super K data to accommodate some $\nu_\mu \rightarrow \nu_e$ at low Δm^2 , as discussed in section 4 below. The ratio-of-ratios, R , for the sub- and multi-GeV data is shown in Fig. 12. Comparing these results to the expectations in Fig. 9, the data are again consistent with oscillations at moderate Δm^2 .

The Soudan Experiment has observed a similar

zenith angle dependence (see contribution by H. Gal- lager). The Soudan detector is a 1 kton fine-grained tracking calorimeter. While this experiment has the drawback of lower statistics than Super K experiment, it has the advantage of the capability to observe the recoil proton in the neutrino interaction. This substantially improves the resolution on θ_z , the angle of the incoming neutrino. At Super K, where only the final state lepton is observed, the average angle between the final state lepton direction and the incoming neutrino direction is 55° at $p = 400 \text{ MeV}/c$ and 20° at $1.5 \text{ GeV}/c$.¹⁷ Using the reconstructed final state particles and the outgoing lepton, the resolution on θ_z for Soudan is 23° for the 200-400 MeV data and 8° for the $> 600 \text{ MeV}$ data.

Neutrinos which travel through the earth may interact in the matter under the detectors. MACRO, Super K and Kamiokande¹⁸ have measured the upward-going muons from these neutrino interactions. All of these experiments see rates below that which is expected and an angular dependence which is consistent with oscillations. In this case, a ratio to ν_e events cannot be used to reduce sensitivity to uncertainties in the ν_μ flux. However, comparisons are made to a wide range for flux models and the ratio has been found to be low in all cases. For example, the MACRO experiment has measured a ratio of data to Monte Carlo of $0.74 \pm 0.036(\text{stat}) \pm 0.046(\text{sys}) \pm 0.013(\text{th})$, which includes the systematic error on the flux calculation. The $\cos\theta_z < 0$ distribution, as reported by D. Michael at ICHEP '98, is consistent with an oscillation hypothesis at moderate Δm^2 . As reported in the same talk, MACRO can also measure upward-going ν_μ interactions within the detector; a deficit in this data, consistent with oscillations, is also observed.

Fig. 13 summarizes the analyses of these experiments under the oscillation hypothesis. Although much attention has been focussed on the fact that the Δm^2 range of Super K extends into the range of 10^{-4} eV^2 , it should be noted that 1) the Super K best fit is consistent with the other results and 2) the Super K R analysis integrated over zenith angle dependence overlaps with the R vs. $\cos\theta_z$ analysis only at the top of the Δm^2 range. Tab. 3 summarizes Δm^2 for the hypothesis that the atmospheric neutrino deficit is entirely explained by $\nu_\mu \rightarrow \nu_\tau$ oscillations. All results are consistent with this oscillation hypothesis. Experiments quote either a "best fit" or a "consistent" Δm^2 value, as noted. As will be noted again in the section on Theoretical Interpretation, the best fits with no $\sin^2 2\theta < 1$ constraint for Super K, Kamiokande and MACRO are all marginally in the unphysical regions, with $\sin^2 2\theta$ of 1.35, 1.05 and > 1.0 , respectively. Taken as a whole, the results are consistent with oscillations $\Delta m^2 \sim 2.5 \times 10^{-3} \text{ eV}^2$ and $\sin^2 2\theta \sim 1$. For a global analysis of the data from the atmospheric neutrino experiments, see the contribution

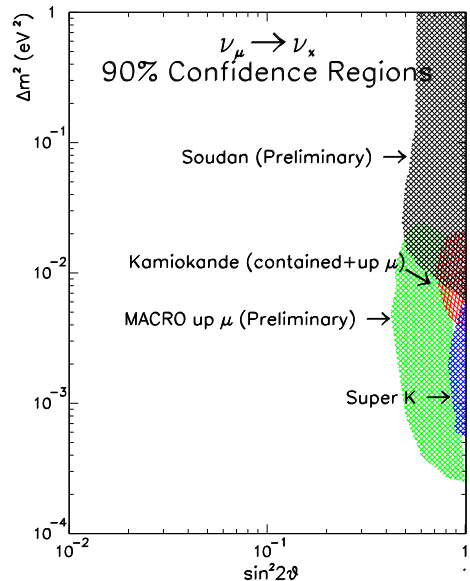


Figure 13: A summary of 90% CL allowed regions for Soudan II, MACRO, Kamiokande and Super K

from Gonzalez-Garcia in these proceedings.

2.3 The LSND Signal

The LSND hint for neutrino oscillations is the only indication for oscillations which is a *signal*, as opposed to a deficit. Evidence has been seen for both $\bar{\nu}_\mu \rightarrow \bar{\nu}_e$ and $\nu_\mu \rightarrow \nu_e$ oscillations. In 1995 the LSND experiment published data showing candidate events that were consistent with $\bar{\nu}_\mu \rightarrow \bar{\nu}_e$ oscillations.¹⁹ Additional event excesses were published in 1996 and 1998 for both $\bar{\nu}_\mu \rightarrow \bar{\nu}_e$ oscillations²⁰ and $\nu_\mu \rightarrow \nu_e$ oscillations.²¹ The two oscillation searches are complementary, having different backgrounds and systematics, yet yielding consistent results.

The experiment is described in the parallel session contribution to these proceedings by R. Imay. This is the only oscillation signature observed from an accelerator experiment, in this case a beam produced at LANCE at LANL, with 800 MeV energy protons interacting with a water target, a close-packed high-Z target and a water-cooled Cu beam dump.

For the decay-at-rest (DAR) analysis ($\bar{\nu}_\mu \rightarrow \bar{\nu}_e$), the beam is produced by π^+ 's which stop and decay in the beam dump, producing muons which then decay to produce $\bar{\nu}_\mu$'s. The signature for oscillations is a $\bar{\nu}_e$ interaction ($\bar{\nu}_e p \rightarrow e^+ n$), yielding a positron signal, followed by $np \rightarrow d\gamma$, where the 2.2 MeV γ is detected. A comparison of the energy dependence of the the observed $\bar{\nu}_e$ events and the non-beam background indicates a "Fitted

Table 4: Preliminary numbers of excess events and the corresponding oscillation probabilities for the running periods 1993-1995, 1996-1997, and 1993-1997.

| Data Sample | Fitted Excess | $\bar{\nu}_e$ Background | Total Excess | Oscillation Probability |
|-------------|------------------|--------------------------|-----------------|------------------------------|
| 1993-1995 | 63.5 ± 20.0 | 12.5 ± 2.9 | 51.0 ± 20.2 | $(0.31 \pm 0.12 \pm 0.05)\%$ |
| 1996-1997 | 35.1 ± 14.7 | 4.8 ± 1.1 | 30.3 ± 14.8 | $(0.32 \pm 0.15 \pm 0.05)\%$ |
| 1993-1997 | 100.1 ± 23.4 | 17.3 ± 4.0 | 82.8 ± 23.7 | $(0.31 \pm 0.09 \pm 0.05)\%$ |

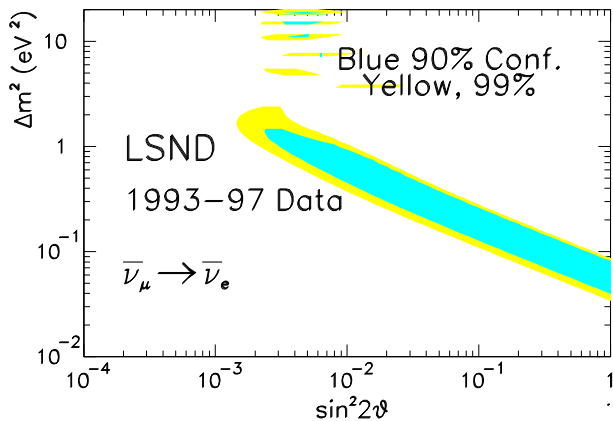


Figure 14: LSND allowed region for data from 1993-1997.

Excess” of events as shown in Tab. 4. Comparing this “Fitted Excess” to the expected $\bar{\nu}_e$ beam background then yields a “Total Excess” for the decay-at-rest analysis, summarized in Tab. 4, and shown by the allowed regions in Fig. 14

The ν_μ ’s in the beam from pion decay-in-flight (DIF) are also used to probe oscillations by the LSND experiment. The signature for $\nu_\mu \rightarrow \nu_e$ oscillations is an electron from the reaction $\nu_e C \rightarrow e^- X$ in the energy range $60 < E_e < 200$ MeV. The excess events are consistent with $\nu_\mu \rightarrow \nu_e$ oscillations with an oscillation probability of $(0.26 \pm 0.10 \pm 0.05)\%$. A fit to the event distributions yields the allowed region in the $(\sin^2 2\theta, \Delta m^2)$ parameter space shown in Fig. 15 (between the solid lines), which is consistent with the allowed region from the $\bar{\nu}_\mu \rightarrow \bar{\nu}_e$ search (dotted lines).

In principle, when discussing signals and limits below, $\bar{\nu}_\mu \rightarrow \bar{\nu}_e$ should be considered separately from $\nu_\mu \rightarrow \nu_e$ to allow for possible CP violation. However, due to the good agreement between the the DAR ($\bar{\nu}_\mu \rightarrow \bar{\nu}_e$) and DIF ($\nu_\mu \rightarrow \nu_e$) data from LSND, and the lack of any other evidence for CP violation in neutrino oscillations, the two cases will be considered together below under the heading “ $\nu_\mu \rightarrow \nu_e$.”

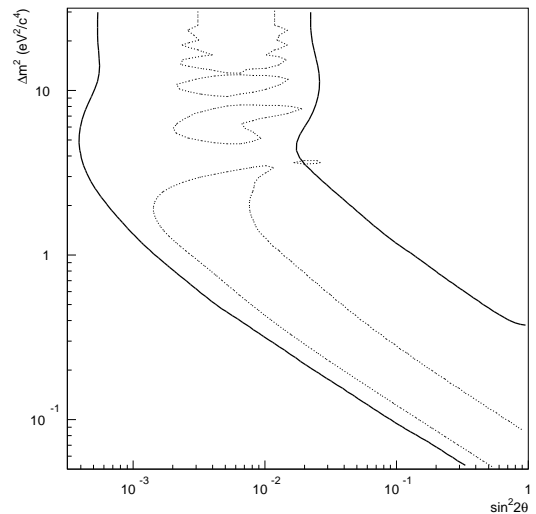


Figure 15: The 95% confidence region for $\nu_\mu \rightarrow \nu_e$ oscillations (solid curve) along with the favored regions for $\bar{\nu}_\mu \rightarrow \bar{\nu}_e$ oscillations (dotted curve).

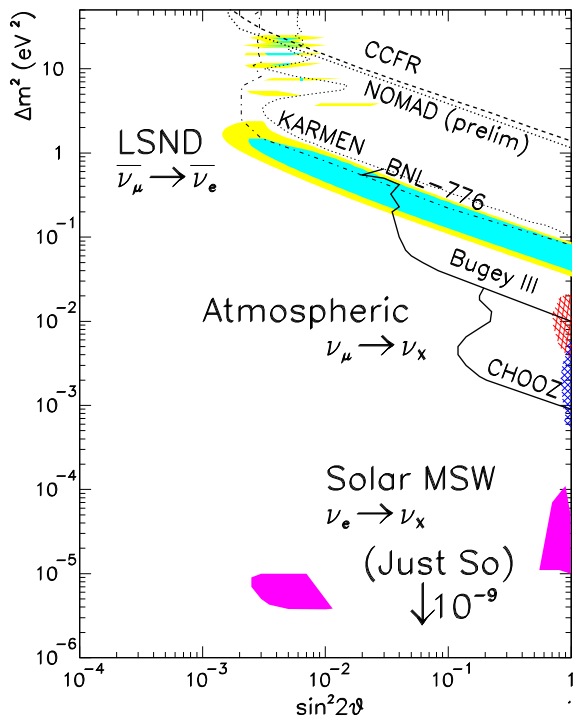


Figure 16: Allowed and excluded regions for $\nu_\mu \leftrightarrow \nu_e$ and $\bar{\nu}_\mu \leftrightarrow \bar{\nu}_e$ oscillations.

3 Experiments Which Set Limits on Oscillations

Many experiments have searched for neutrino oscillations and seen no signal. Tab. 5 provides a list of the exclusion experiments whose results appear in this section. Results from CCFR/NuTeV, Nomad, CHORUS and KARMEN 2 are reviewed in these proceedings by R. Drucker, D. Autiero, P. Migliozzi and J. Kleinfeller, respectively.

3.1 Limits on $\nu_\mu \leftrightarrow \nu_e$ oscillations

In principle, all three indications of oscillations can be interpreted as $\nu_\mu \leftrightarrow \nu_e$. If the solar deficit is due to oscillations, it is entirely $\nu_e \rightarrow \nu_X$, where ν_X may be ν_μ (or ν_τ , as discussed later). Because of the very low Δm^2 associated with all models for solar neutrino oscillations, no terrestrial neutrino experiment has been able to directly test the $\nu_e \rightarrow \nu_\mu$ hypothesis. The atmospheric deficit appears to be largely $\nu_\mu \rightarrow \nu_X$, where ν_X could be ν_e . However, this is regarded as unlikely for two reasons. First, the Super K fits to the combination of “e-like” (ν_e candidate) and “ μ -like” (ν_μ candidate) events give a poor χ^2/DOF of 87.8/67 for describing the data as entirely $\nu_\mu \leftrightarrow \nu_e$ (see contribution by McGrew, these proceedings). Furthermore, the reactor experiments, Bugey²³

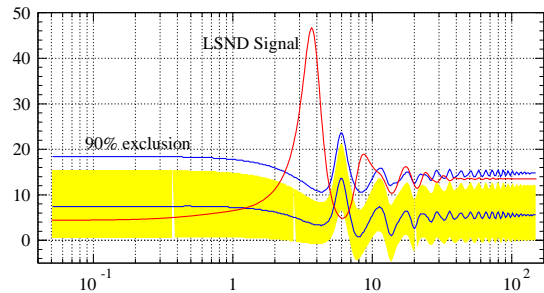


Figure 17: The KARMEN 1 excess is the central line, with one sigma shaded errors bars, shown as a function of Δm^2 . The LSND expectation is superimposed.

and CHOOZ²⁴ which search for ν_e disappearance, have excluded nearly all of the allowed region for atmospheric $\nu_\mu \leftrightarrow \nu_e$. The 90% exclusion regions from these experiments are indicated on Fig. 16. LSND is required to be $\bar{\nu}_\mu \rightarrow \bar{\nu}_e$, because it is an observed signal. This signal is the most amenable to systematic study at accelerators due to the larger Δm^2 values involved: $> 0.1 \text{ eV}^2$ compared to $10^{-2} - 10^{-3} \text{ eV}^2$ for the atmospheric neutrino problem and $10^{-4} - 10^{-5} \text{ eV}^2$ for the solar neutrino problem. Thus in studying the LSND signal, detectors can be placed much closer to the neutrino source and higher energy neutrino beams can be used. The high Δm^2 region has been excluded by the Nomad (preliminary) and CCFR results.²⁵ Therefore, interest is now focussed on the $\Delta m^2 = 0.1$ to 1.0 eV^2 region.

The KARMEN experiment²⁶ is complementary to LSND, running at the ISIS facility in Rutherford, England, with a neutrino source produced by pion decay-at-rest. The detector is smaller than LSND and the beam is less intense than at LANCE, resulting in lower statistics than LSND by $\sim \times 10$. The KARMEN 1 experiment took data through 1995.

KARMEN 1 observed an excess of approximately seven events, which is in agreement with predictions based on the LSND central values at low Δm^2 .²⁶ The measured KARMEN 1 excess, as a function of Δm^2 , is shown in Fig. 17. The shaded band showing the error associated with the measurement indicates that the excess is only at the 1σ level. However, the overall excess is in agreement with the central allowed value of LSND at low Δm^2 . The LSND prediction is indicated by the labeled line in Fig. 17. In the region of $\Delta m^2 < 1 \text{ eV}^2$, the LSND central prediction of 4 events is in good agreement with the observed excess of 7 events. Because of the low significance of the excess, KARMEN collaboration prefers to quote a limit for their first-run result, with the number of events set by the “90% exclusion” line shown in

Table 5: Some of the recent experiment which have set limits on oscillations. Regions ruled out by these experiments are discussed in section 3. Under “reference”, listed names refer to contributions to these proceedings.

| Experiment | Source/Beam | $\sim E_\nu$ | $\sim L$ | Detector | Ref. |
|-------------|---------------------------------|--------------|-------------|--|-----------------|
| CCFR/NuTeV | accel. $\nu_\mu, \bar{\nu}_\mu$ | 100 GeV | 1 km | Iron/scint cal and muon spect | 25, Drucker |
| Nomad | accelerator ν_μ | 26 GeV | 1 km | DC targ. w/i mag., EM cal, TRD | Autiero |
| CHORUS | accelerator ν_μ | 26 GeV | 1 km | Emuls. targ. w/ scint fiber, tracking, cal | Migliozzi |
| CDHS | accelerator ν_μ | 1 GeV | 1 km | Iron/scint cal and muon spect | 29 |
| BNL E776 | accelerator ν_μ | 1.4 GeV | 1 km | Concrete/DC cal and muon spect | 22 |
| KARMEN 1, 2 | π DAR $\bar{\nu}_\mu$ | 20-60 MeV | 17 m | Liquid Scint Detector | 26, Kleinfeller |
| CHOOZ | reactor $\bar{\nu}_e$ | 3 MeV | 1 km | Gd-doped scintillator oil | 24 |
| Bugey | reactor $\bar{\nu}_e$ | 3 MeV | 15, 40, 95m | Gd-doped scintillator oil | 23 |

Fig. 17. The KARMEN 1 limit appears in Fig. 16 .

As reported at this conference (see contribution by J. Kleinfeller), the second run of the KARMEN experiment (KARMEN 2) is in progress. Due to upgraded shielding, the cosmic ray background has been significantly reduced. At this point, $\sim 40\%$ of the data have been collected. The background expected for this running period is 3 events, and a typical signal for the $\Delta m^2 < 1 \text{ eV}^2$ region is 1 event, if LSND is correct. The total number of events observed during this period (combined signal and background) is zero (which has a 5.6% probability of occurring as a statistical fluctuation).

The quandary associated with the treatment of data in this situation has already been discussed above in section 1. The limit which can be set in the situation where an experiment fails to see the expected background will be better than the actual experimental sensitivity, that is, the expectation if the background had been observed. Fig. 2 shows various interpretations of the KARMEN 2 null result. The Bayesian approach, the Feldman-Cousins method and the Giunti Method give differing limits, thus making the result hard to interpret. The sensitivity of KARMEN 2 is shown by the lines connected with open symbols. The sensitivity is worse than BNL 776 and does not cover the LSND signal region.

At this point, the situation for $\nu_\mu \leftrightarrow \nu_e$ oscillations in the LSND region can be summarized in the following manner. Three results show excesses:

- 33.9 ± 8.0 events (LSND Decay-at-rest, $\bar{\nu}_\mu \rightarrow \bar{\nu}_e$)
- 18.1 ± 6.6 (LSND Decay-in-flight, $\nu_\mu \rightarrow \nu_e$)
- 7.3 ± 7.0 (KARMEN 1 Decay-at-rest, $\nu_\mu \rightarrow \nu_e$)

One experiment (KARMEN 2) which expected 3 events background, plus one event signal, has observed zero total events.

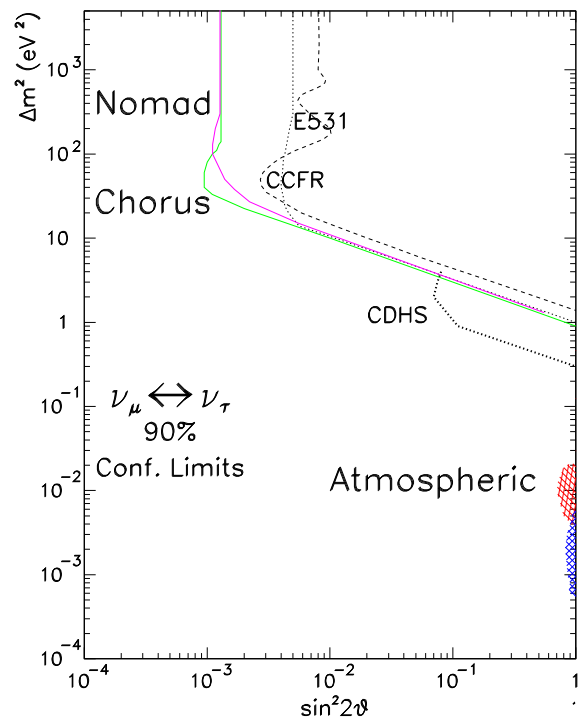


Figure 18: Status of $\nu_\mu \rightarrow \nu_\tau$ oscillation searches.

3.2 Limits on $\nu_\mu \leftrightarrow \nu_\tau$ oscillations

The CHORUS and NOMAD experiments²⁷ explore the high Δm^2 $\nu_\mu \leftrightarrow \nu_\tau$ oscillation region, where one may expect a signature from neutrinos which contribute to “dark matter” in the universe. Recent astrophysical data has indicated that some of the dark matter may be “hot.” One candidate for hot dark matter is massive neutrinos. Present data can accommodate $\Omega = 0.1 \sim 0.4$ with $\Omega_{HDM} < 0.2$, as reviewed by B. Kayser at this conference. Massive neutrinos may be an important component of the dark matter in the universe since the density of relic neutrinos from the Big Bang is $\sim 100 \nu\text{'s/cm}^3/\text{type}$. Neutrinos in the mass range of $1 \sim 6 \text{ eV}$ could help to explain the small scale structure in the universe and recent anisotropy measurements of the photon background radiation²⁸. If one assumes that the heaviest neutrino is much more massive than the rest, then the astrophysical data indicate that the region of interest for searches is approximately $1 < \Delta m^2 < 36 \text{ eV}^2$.

NOMAD and CHORUS share a high-intensity ν_μ beam produced at CERN. The neutrino energies range from $10 \sim 40 \text{ GeV}$. The $\bar{\nu}_\mu$ contamination in this beam is only $\sim 5\%$. The prompt ν_τ contamination is $(3 \pm 4) \times 10^{-6}$.

The CHORUS experiment uses an 800 kg emulsion target which provides $< 1 \mu\text{m}$ spatial resolution. Thus this experiment can identify ν_τ charged current interactions by seeing the τ decay in the emulsion after a few tenths of a millimeter, producing a kink in the track. Automatic emulsion scanning systems have been developed to handle the large quantities of data ($\sim 300,000$ events). The emulsion target is followed by a magnetic spectrometer, calorimeter and muon spectrometer allowing momentum reconstruction and particle identification in each event.

NOMAD is a fine-grained electronic detector composed of a large aperture dipole magnet ($3m \times 3m \times 7m$ with $B = 0.4 \text{ T}$) filled with drift chambers that act as both the target and tracking medium. The experiment uses kinematic cuts associated with the missing energy from outgoing $\nu\text{'s}$ in the τ decay to separate statistically a possible oscillation signal.

CHORUS and NOMAD experiments have sensitivity to oscillations with $\Delta m^2 > 1 \text{ eV}^2$. Preliminary negative search results are reported for approximately $\sin^2 2\theta > 2 \times 10^{-3}$, as shown in Fig. 18. Because no signal has been observed in these experiments, the possibility that massive neutrinos are dark matter is becoming more unlikely. However, it remains possible that the mixing is very small; thus the possibility is not entirely ruled out.

Among the hints for oscillations discussed previously, only the atmospheric neutrino deficit may result from $\nu_\mu \leftrightarrow \nu_\tau$ oscillations. The Δm^2 reach of the present

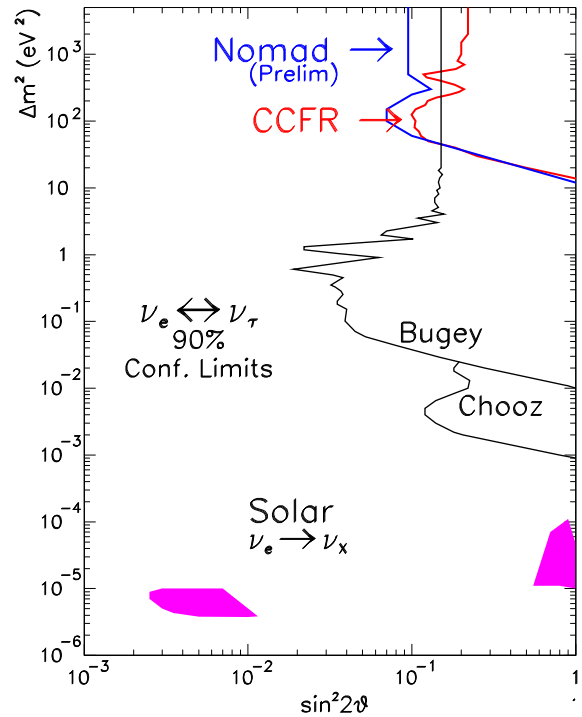


Figure 19: Status of $\nu_e \rightarrow \nu_\tau$ oscillation searches.

experiments does not cover the atmospheric allowed region. The lowest limit, $\Delta m^2 \sim 0.3 \text{ eV}^2$ is from the CDHS experiment.²⁹

3.3 Limits on $\nu_e \leftrightarrow \nu_\tau$ oscillations

Naively, $\nu_e \rightarrow \nu_\tau$ oscillations appear least likely, because this skips the second generation. However, this oscillation does appear in some models, as discussed in section 4. The one hint which can be interpreted as such an oscillation is the solar neutrino deficit. In addition, one or more of the neutrinos may represent a fraction of the dark matter in the universe. If there is a mass difference between the neutrinos, this might manifest itself through $\nu_e \rightarrow \nu_\tau$ oscillations at relatively high Δm^2 .

The excluded regions for $\nu_e \rightarrow \nu_\tau$ are shown in Fig. 19, along with the solar allowed region. Recent searches from NOMAD and CCFR have addressed high $\Delta m^2\text{'s}$, while the reactor experiments have explored down to 10^{-3} eV^2 . The terrestrial experiments remain a few orders of magnitude away from addressing the solar $\nu_e \rightarrow \nu_\tau$ hypothesis.

4 Theoretical Interpretation of the Data

When comparing the evidence for oscillations with the excluded regions, we are faced with theoretical problems with both the suggested Δm^2 regions and the mixing

angles. There are apparently three distinct Δm^2 regions:

$$\begin{aligned}\Delta m_{solar}^2 &= 10^{-5} \text{ or } 10^{-10} \text{ eV}^2 \\ \Delta m_{atmos}^2 &= (10^{-2} \text{ to } 10^{-4}) \text{ eV}^2 \\ \Delta m_{LSND}^2 &= (0.2 \text{ to } 2) \text{ eV}^2\end{aligned}$$

However, in a straightforward three-generation mixing model, if Δm_{12}^2 is very small, then $\Delta m_{13}^2 \approx \Delta m_{23}^2$, leading to only two apparent Δm^2 regions. Furthermore, one must address the very large mixing in the neutrino sector compared to the quark sector. For the atmospheric data there is no solution at 90% CL with $\sin^2 2\theta$ less than approximately 0.6.

The problem has been attacked in several ways. Several possibilities are presented in these proceedings by B. Kayser, M. Gonzalez-Garcia, S. Nandi, and P. Roy. Some phenomenologists choose to admit complications in the simplistic three generation mixing model. Others prefer to introduce a sterile neutrino. Some like to throw out the data which they like the least. The first two options merit further explanation.

4.1 Three Generation Mixing Models

If three generation mixing is to explain all of the data, then one of the following must be true:

- $\Delta m_{solar}^2 \approx \Delta m_{atmos}^2$
- $\Delta m_{LSND}^2 \approx \Delta m_{atmos}^2$
- Δm_{atmos}^2 is a convolution of Δm_{solar}^2 and Δm_{LSND}^2 .

The first two possibilities are difficult to accommodate. As shown in Fig. 3, the three allowed regions are well separated, although one should keep in mind that these plots show only 1.3σ regions. The third possibility is now under exploration and will be considered here.

With three generations of neutrinos, one would expect a more complicated oscillation phenomenology that includes transitions between all pairs. In this case, an experiment which observes ν_μ disappearance, like Super K, may be seeing a combination of $\nu_\mu \rightarrow \nu_\tau$ and $\nu_\mu \rightarrow \nu_e$. If one then takes the data and analyzes it in terms of only one scenario, for example only $\nu_\mu \rightarrow \nu_\tau$, then one will extract a Δm^2 which is some convolution of the two real Δm^2 regions. It is interesting to note that this could also lead to a best fit for $\sin^2 2\theta$ which is greater than one, as has been observed by the atmospheric experiments.

For this to be an acceptable hypothesis, the Super K data must accommodate $\nu_\mu \rightarrow \nu_e$ oscillations at low Δm^2 . As shown in Fig. 9, low Δm^2 oscillations will only be apparent in the most negative $\cos\theta_z$ bins. The Super

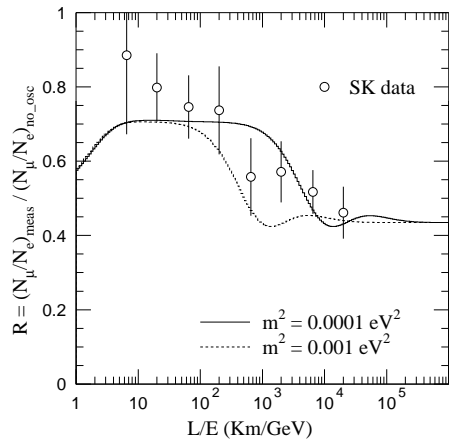


Figure 20: Fits to the Super K atmospheric ratio-of-ratios, R , assuming contributions from $\nu_\mu \rightarrow \nu_\tau$ at $\Delta m^2 = 0.4 \text{ eV}^2$ and $\nu_\mu \rightarrow \nu_e$ at low Δm^2 .

K data, shown in Fig. 11 may see an excess in the lowest $\cos\theta_z$ bin of the “e-like” data. Therefore, it may be possible to fit the Super-K data with an admixture of $\nu_\mu \rightarrow \nu_\tau$ and $\nu_\mu \rightarrow \nu_e$.

As an example, Thun and McKee have presented³⁰ an explanation for the data assuming three generation mixing with $\Delta m_1^2 = 0.4 \text{ eV}^2$ and $0.0001 < \Delta m_2^2 < 0.001 \text{ eV}^2$. The mixing matrix describing the oscillation (see equation 2) is

$$\begin{pmatrix} \nu_e \\ \nu_\mu \\ \nu_\tau \end{pmatrix} = \begin{pmatrix} 0.78 & 0.60 & 0.18 \\ -0.61 & 0.66 & 0.44 \\ 0.15 & -0.45 & 0.88 \end{pmatrix} \begin{pmatrix} \nu_1 \\ \nu_2 \\ \nu_3 \end{pmatrix}$$

This choice of parameters makes certain predictions for each of the three indications of neutrino oscillations:

atmospheric data – Using $\Delta m_2^2 = 3 \times 10^{-4} \text{ eV}^2$ for an example, this model predicts the ratio-of-ratios for the atmospheric data to be 0.72, which is consistent with the experimental average of $\sim 0.6 \pm 0.1$. As shown in Fig. 20, the model fits the $\cos\theta_z$ dependence of the Super K R reasonably well for the quoted range of Δm_2^2 , although the normalization appears to be low. This fit would improve if the higher Δm^2 value were chosen to be 0.2 eV^2 , leading to a shift upward in the overall normalization.

solar data – The Thun-McKee solution predicts that the ratio of data to Monte Carlo in the solar experiments should be 0.5 for all experiments. For this to be correct, then the Homestake experiment would have to be observing a ratio which has fluctuated low by 3.1σ if the BP98 (SSM) model is used. However, if the ratio is taken using the Turck-Chieze and Lopes solar model³¹, then one obtains $0.403 \pm 0.025 \pm 0.025$ which is in agreement with the Thun-McKee assumption of 0.5. The choice of large-mixing angle solar solution is somewhat dis-

avored unless one introduces an increase in the *hep* neutrinos, as discussed in section 2, above.

LSND data – The choice of $\Delta m^2 = 0.4 \text{ eV}^2$ and $\sin^2 2\theta_{eff} = 0.026$ for LSND is within the allowed region, although extremely close to the Bugey 90% CL limit. These parameters indicate that the KARMEN 1 experiment would see 3 event excess, which is consistent with the measured 7 event excess. For the total KARMEN 2 running, this model predicts a 2 event excess, hence to date less than 1 event is expected. At this point, KARMEN 2 has failed to observe either an excess or the expected three background events (see section 3).

There is no quoted overall χ^2 for the Thun and McKee (nor any other) three-generation model.

It is important to recognize that Thun and McKee have not fit the data. They have simply chosen a set of parameters and demonstrated that it is possible to develop a model which fits much of the experimental data. Other models of three generation mixing have also been developed based on a clever choice of parameters which also come close to fitting all of the data.³² In every case, there are experimental issues which make the choice of parameters uncomfortable. A global analysis, which incorporates all of the data including systematic errors and correlations, similar to the fits done to obtain the electroweak parameters, is needed.

4.2 Sterile Neutrinos

The second option for fitting the experimental data is to introduce a sterile neutrino. The sterile neutrino ν_s does not interact through the weak interaction because it is postulated to be an isosinglet partner to the “standard light neutrinos.” Thus oscillations between a ν_e , ν_μ or ν_τ and a ν_s would cause the standard neutrino to apparently disappear. Obviously sterile neutrinos can only be invoked for cases where a deficit (as opposed to a signal) are observed. So sterile neutrinos may provide the explanation for the atmospheric or solar deficits, but LSND is required to be $\nu_\mu \rightarrow \nu_e$.

Sterile neutrinos were first proposed as an explanation for the solar deficit by Caldwell and Mohapatra³³ in 1993. A more recent example is the model by Barger, Weiler and Whisnant.³⁴ In this picture, the solar deficit is explained by $\nu_e \rightarrow \nu_s$ oscillations. The atmospheric deficit is $\nu_\mu \rightarrow \nu_\tau$.

Alternatively, the atmospheric result may be largely $\nu_\mu \rightarrow \nu_s$, as suggested by Joshipura and Smirnov³⁵. The solar data can then be explained as a combination of $\nu_e \rightarrow \nu_\tau$ and $\nu_e \rightarrow \nu_s$.

The sterile neutrino has several nice features. By adding an extra degree of freedom (the mass of the ν_s)

to the theory, one can comfortably fit all of the data. The ν_s provides an isosinglet for grand unified theories, however the apparent light mass of the ν_s presents difficulties. The extremely large apparent mixing angles can be explained by arguing that the $\nu_e \leftrightarrow \nu_\mu \leftrightarrow \nu_\tau$ mixings are comparable to the quark sector while mixing to ν_s is large. Finally, the ν_s is a candidate for hot dark matter.

5 Future Experiments

The existing indications of neutrino oscillations raise many questions for future experiments to address. Many new experiments are proposed to address the issues which have been raised by the present data. This section provides an overview of some of the exciting results which can be expected in the near future.

5.1 Future Tests of Solar Neutrino Oscillations

The issues related to the solar neutrino deficit are:

- Can we see the L/E dependence which will clearly demonstrate neutrino oscillations?
- Is this $\nu_e \rightarrow \nu_\mu$, ν_τ or ν_s (or some combination)?
- What is the Δm^2 ? Is MSW or Just-So the right explanation?
- If the solution is MSW, is it the small or large angle solution?
- Is there any room for doubting the Standard Solar Model?

In order to address the L/E dependence, a wide range of experiments with varying energy thresholds is needed. Tab. 6 provides a summary of the upcoming solar experiments which were presented at ICHEP’98 (see contributions by C. Waltham, M. Chen, T. Patzak, D. Vignaud and Y.F. Wang, these proceedings). As can be seen from the Tab. 6 these and other proposed future experiments will cover energies ranging upward from 0.05 MeV, permitting tests of the L/E dependence.

The BOREXINO experiment³⁶ is sensitive to neutrinos from the ${}^7\text{Be} + e^- \rightarrow {}^7\text{Li} + \nu_e$ interaction, which is a delta function in the flux distribution, as shown on Fig. 5. Therefore, this experiment will be highly sensitive to seasonal variations in L , the earth-sun distance, if the “Just So” solution is correct.

The SNO experiment³⁷ will test the hypothesis for sterile neutrino solar oscillations. This experiment observes neutral current (NC) interactions for all three standard neutrinos and charged current (CC) ν_e interactions. Sterile neutrinos will not have neutral current interactions. Therefore the ratio of NC to CC interaction

Table 6: Some future Solar Neutrino Experiments

| Experiment | Detector | Search | Source | Approx. Range |
|------------|---------------|--|----------|-----------------------------|
| SNO | Deuterium | $\nu_x + d \rightarrow p + n + \nu_x$ (NC $x = e, \mu, \tau$) types) $\nu_e + d \rightarrow p + p + e^-$ (CC ν_e only) | Sun | $> 5 \text{ MeV}$ |
| BOREXINO | Liquid Scint. | ν_e elastic scatters | Sun | $0.5 < E < 1.0 \text{ MeV}$ |
| GNO | Gallium | ν_e capture in Ga | Sun | $> 0.2 \text{ MeV}$ |
| HELLAZ | Helium TPC | ν_e elastic scatters | Sun | $> 0.05 \text{ MeV}$ |
| KamLAND | Liquid Scint. | ν_e elastic scatters | Reactors | $> 1 \text{ MeV}$ |

rates will be lower than predicted if solar oscillations are $\nu_e \rightarrow \nu_s$.

As the only terrestrial experiment which can address the solar neutrino question, the KamLAND experiment³⁸ is not affected by theoretical errors from the Standard Solar Models. This experiment will be located in the Kamiokande cavern and will make use of neutrinos from five reactor sites, resulting in $L \sim 160 \text{ km}$. This experiment is sensitive only to the LMA MSW solution.

In the far future, an interesting test of LMA MSW $\nu_e \rightarrow \nu_\tau$ and $\nu_e \rightarrow \nu_\mu$ oscillations may be made by the first stage of the muon collider. A muon storage ring would provide an intense beam of ν_e 's (and ν_μ 's) from muon decays. Using a 50 GeV storage ring and beams directed from the US to Italy and Japan, single event sensitivity covers the upper region of the LMA solution.³⁹

5.2 Future Tests of Atmospheric Neutrino Oscillations

The issues related to the atmospheric neutrino deficit are:

- Can we see an effect in the controlled environment of an accelerator experiment?
- Is this mainly $\nu_\mu \rightarrow \nu_\tau$ or ν_s (or some combination)?
- Is there any $\nu_\mu \rightarrow \nu_e$ component?
- What is the Δm^2 ?

It is possible to be sensitive to the moderate Δm^2 's indicated by the atmospheric neutrino deficit through "long baseline" experiments. In the near future, beams will be built at accelerator facilities with $E_\nu \sim 1 - 10 \text{ GeV}$ which point to detectors at distances of hundreds of kilometers. This opens a new era of tests of neutrino oscillations in the atmospheric region, with entirely different systematics from the previous experiments.

The sensitivities of two long baseline experiments which are approved to run in the near future are shown in Fig. 21. The K2K experiment, which uses a 250 km baseline from KEK to the Super K detector, will begin taking data in 1999. The MINOS experiment, with a 730 km baseline from FNAL to Minnesota, will begin taking data

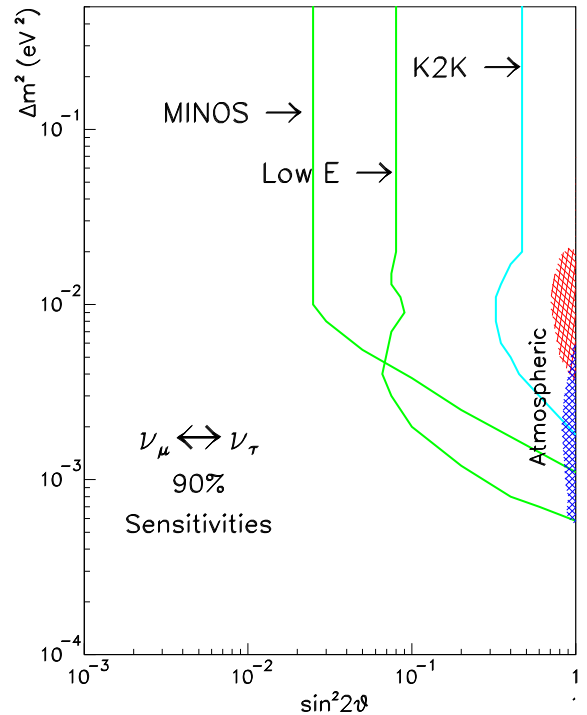


Figure 21: Sensitivities for MINOS and K2K, two long baseline experiments approved to run in the near future. MINOS is also considering running with a low energy ("Low E") beam design.

in 2002. The 90% CL expectations for ν_μ disappearance are shown in Fig. 21. The MINOS experiment has both a “standard” and “low energy” beam configuration, as indicated by the two lines. Each of these experiments has a near detector to measure the initial beam flux. The far detectors are sensitive to ν_μ disappearance and ν_e appearance. The K2K experiment is sensitive to the full Kamiokande allowed region.⁴⁰ If the three generation mixing scenario with $\Delta m^2 \sim 0.3 \text{ eV}^2$ $\nu_\mu \rightarrow \nu_\tau$ oscillations is correct, then K2K will see a deficit. The MINOS “standard beam” configuration covers the region where all of the atmospheric experiments overlap at greater than 5σ . Full coverage of the Super K region is obtained with the “low energy” beam configuration.⁴¹

CERN is in the process of planning an extensive long baseline program using a beam directed to the Gran Sasso facility. The richness of this program lies in the diversity of detectors, addressing important issues of systematics and allowing both appearance and disappearance studies. The ICARUS experiment has been approved and is presently under construction. The 600 ton liquid argon calorimeter, to be completed in 2000, will be sensitive to ν_μ disappearance and ν_e appearance.⁴² The NOE experiment, consisting of scintillating fibers alternating with TRD detectors, also will have ν_μ disappearance and ν_e appearance capabilities.⁴³ The AQUARICH experiment proposes a 27-kton water target/ring-imaging Cerenkov detector, allowing a search for ν_μ disappearance.⁴⁴ The baseline from CERN to the Gran Sasso is 740 km. Various beam energy options are under discussion.

Perhaps the most exciting future possibilities lie with experiments which can detect τ 's produced in $\nu_\mu \rightarrow \nu_\tau$ oscillations. Observation of a significant signal would be decisive. The most promising detector technology for τ identification is emulsion. Using a beam dump neutrino source, the DONUT (“Discovery Of the NU Tau”) Experiment at FNAL recently identified several ν_τ interaction candidates, thus possibly providing the first direct observation of ν_τ and also demonstrating the capability of hybrid emulsion detectors.⁴⁵ A candidate ν_τ event is shown in Fig. 22. The MINOS experiment using the FNAL beam and the OPERA experiment using the CERN beam are considering running with ~ 1 kton emulsion detectors. Using MINOS as an example, one would expect 7 events at $\Delta m^2 = 1 \times 10^{-3} \text{ eV}^2$ in two years of running with the standard beam configuration.

The TOSCA experiment at CERN is a proposed short baseline emulsion experiment. This experiment is exploring $\nu_\mu \rightarrow \nu_\tau$ oscillations in the high Δm^2 region. It was originally motivated by the hot dark matter neutrino scenario. If TOSCA were to observe oscillations in the $\Delta m^2 > 1 \text{ eV}^2$ and small mixing angle region, this would render $\nu_\mu \rightarrow \nu_s$ the most likely explanation for the

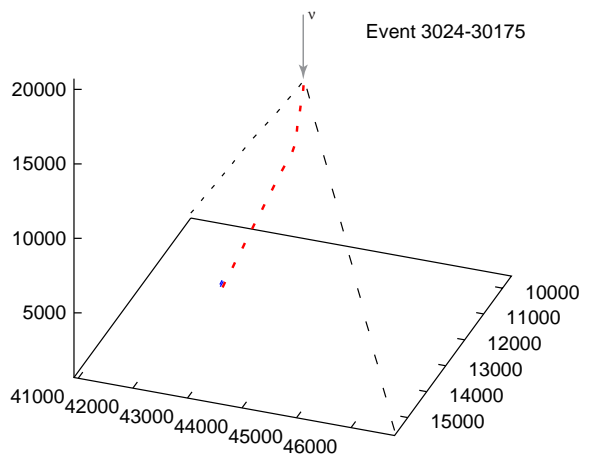


Figure 22: ν_τ interaction candidate observed by the DONUT experiment at Fermilab. The neutrino vector is indicated by the arrow. The interaction produced three tracks in the emulsion. One track shows a distinct kink, which is the signature of a τ decay.

atmospheric neutrino deficit. TOSCA will have sensitivity down to $\Delta m^2 \sim 0.4 \text{ eV}^2$ region, also allowing this experiment to investigate three-generation mixing models incorporating the atmospheric result, such as the one proposed by Thun and McKee (see section 4).

5.3 Future Tests of the LSND Signal

The issues related to the LSND signal are:

- Is the signal due to oscillations?
- What is the Δm^2 ?
- What is the $\sin^2 2\theta$?

At this point enticing signals have been seen in three types of experiments exploring this channel (see section 2). What is required at this point is an experiment which definitively covers the entire LSND allowed region at $> 5\sigma$ and which can accurately measure the oscillation parameters.

BooNE (Booster Neutrino Experiment), which has been approved at FNAL, will be capable of observing both $\nu_\mu \rightarrow \nu_e$ appearance and ν_μ disappearance. The first phase, MiniBooNE, is a single detector experiment designed to obtain ~ 1000 events per year if the LSND signal is due to $\nu_\mu \rightarrow \nu_e$ oscillations. This establishes the oscillation signal at the $\sim 8\sigma$ level. The second phase

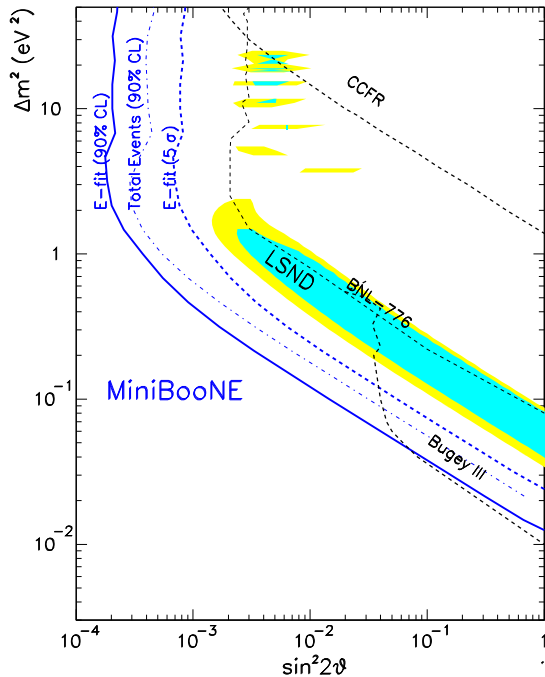


Figure 23: Sensitivity regions for the MiniBooNE experiment with 5×10^{20} protons on target (1 year). The solid (dashed) curve is the 90% CL (5σ) region using the energy fit method and the dashed-dot curve is the 90% CL region using the total event method.

of the experiment introduces a second detector, with the goal to accurately measure the Δm^2 and $\sin^2 2\theta$ parameters of observed oscillations.

The MiniBooNE experiment⁴⁶ (phase 1 of BooNE) will begin taking data in 2001. The detector will consist of a spherical tank 6 m in radius. An inner structure at 5.5 m radius will support 1220 8-inch phototubes (10% coverage) pointed inward and optically isolated from the outer region of the tank. The vessel will be filled with 769 ton of mineral oil, resulting in a 445 ton fiducial volume. The outer volume will serve as a veto shield for identifying particles both entering and leaving the detector, with 292 phototubes mounted on the support structure facing outwards. The first detector will be located 500 m from the Booster neutrino source. The neutrino beam, constructed using the 8 GeV proton Booster at FNAL, will have an average beam energy of approximately 0.75 GeV.

The sensitivity to oscillations can be calculated by summing over energy or by including energy dependence in the fit. As shown in Fig. 23, both the summed analysis and the energy-dependent analysis extend well beyond the LSND allowed region at 90% CL. Also shown is the region where MiniBooNE will see a 5σ or greater signal above background and make a conclusive measurement, which again extends well beyond the LSND signal region.

6 Conclusions

The results which were presented in parallel session 2 on neutrino oscillations are both exciting and confusing. The three hints for neutrino oscillations – solar, atmospheric and LSND – are all at the edge of being conclusive. If confirmed, this would mean that neutrinos have mass and that lepton number is not completely conserved – thereby changing our understanding of the Standard Model. Yet we cannot explain why there should be three significantly different Δm^2 regions. Nor do we understand the large mixing angles. We may be observing oscillations to an entirely new particle, the sterile neutrino. Many new measurements are planned or underway and have the goal to tell definitively if any of the hints are indeed associated with neutrino oscillations. There is much left to learn before we agree on the answers to the questions presented at ICHEP'98. But one thing is without question: these are exciting times for physics!

Acknowledgements

Thanks to all of the speakers from ICHEP '98 Parallel Session 2, and to Bill Louis and Mike Shaevitz.

References

1. R. M. Barnett, *et. al.*, E. Phys. J. C **3** 23 (1998).
2. For example, R. M. Barnett, *et. al.*, Phys. Rev. D **54**, 162 (1996).
3. G. J. Feldman and R. D. Cousins, Phys. Rev. D **57** 3873 (1998).
4. C. Giunti, hep-ph/9808240, (1998).
5. J.N. Bahcall, S. Basu and M. H. Pinsonneault, Phys. Lett. B **433** 1 (1998).
6. R. Davis, Prog. Part. Nucl. Phys. **32**, 13 (1994).
7. J. N. Abdurashitov *et. al.*, Phys. Lett. B **328**, 234 (1994); P. Anselmanni *et. al.*, Phys. Lett. B **328**, 377 (1994).
8. Y. Fukuda *et. al.*, Phys. Rev. Lett. **77** 1683 (1996).
9. J. N. Bahcall and P. I. Krastev, Phys. Lett. B **436** (243) 1998.
10. E. G. Adelberger *et. al.*, "Solar Fusion Cross Sections," To be published in Rev. Mod. Phys., Oct. 1998, astro-ph/9805121.
11. For example, J. Christensen-Dalsgaard *et. al.*, Science **272** 1286 (1996).
12. For example, Castellani *et. al.*, Nucl. Phys. Proc. Suppl. **70** 301 (1998).
13. N. Hata and P. Langacker, Phys. Rev. D **56** 6107 (1997); N. Hata and P. Langacker, Phys. Rev. D **50**, 632 (1994).

14. L. Wolfenstein, Phys. Rev. D17, 2369 (1978); D20, 2634 (1979); S. P. Mikheyev and A. Yu. Smirnov, Yad. Fiz. 42, 1441 (1985) [Sov. J. Nucl. Phys. 42, 913 (1986)]; Nuovo Cimento 9C, 17 (1986).
15. J.N. Bahcall, P.I. Krastev, and A. Yu. Smirnov, hep-ph/9807216, submitted to Phys. Rev. D.
16. Y. Hirata *et al.*, Phys. Lett. **B335**, 237 (1994).
17. Y. Fukuda *et al.*, Phys. Rev. Lett. **81** 1158 (1998).
18. S. Hatakeyama *et al.*, Phys. Rev. Lett **81** 2016 (1998).
19. C. Athanassopoulos *et al.*, Phys. Rev. Lett. **75**, 2650 (1995);
20. C. Athanassopoulos *et al.*, Phys. Rev. Lett. **77**, 3082 (1996); C. Athanassopoulos *et al.*, Phys. Rev. C. **54**, 2685 (1996).
21. C. Athanassopoulos *et al.*, LA-UR-97-1998, submitted to Phys. Rev. C.
22. L. Borodovsky *et al.*, Phys. Rev. Lett. **68**, 274 (1992).
23. B. Achkar *et al.*, Nucl. Phys. **B434**, 503 (1995).
24. M. Apollonio *et al.*, hep-ex/9711002, submitted to Phys. Lett. B.
25. A. Romosan *et al.*, Phys. Rev. Lett. **78** 2912 (1997).
26. B. Bodmann *et al.*, Phys. Lett. B **267**, 321 (1991); B. Bodmann *et al.*, Phys. Lett. B **280**, 198 (1992); B. Zeitnitz *et al.*, Prog. Part. Nucl. Phys., **32** 351 (1994). K. Eitel, hep-ex/9706023.
27. CHORUS WWW Site: <http://choruswww.cern.ch/>
NOMAD WWW Site: <http://nomadinfo.cern.ch/>
28. J.R. Primack, *et al.*, Phys. Rev. Lett. **74** (1995) 2160.
29. F. Dydak *et al.*, Phys. Lett. B **134**, 281 (1984).
30. R.P. Thun and S. McKee, hep-ph/9806534, submitted Phys. Lett. B.
31. S. Turck-Chieze and I. Lopes, Astrophys. J. **108** (1993).
32. Two other examples are: G. Barenboim and F. Scheck, hep-ph/9808327; T. Teshima and T. Sakai, hep-ph/9805386.
33. D.Caldwell and R. Mohapatra, Phys. Rev. D **48** 3259 (1993).
34. V. Barger, T.J. Weiler, and K. Whisnant, hep-ph/9807319 (1998).
35. A. S. Joshipura and A.Yu. Smirnov, hep-ph/9806376.
36. See <http://almime.mi.infn.it/>
37. See <http://www.sno.phy.queensu.ca/>
38. Y. F. Wang, STANFORD-HEP-98-04 (1998). P. Alivisatos *et al.*, STANFORD-HEP-98-03 (1998).
39. S. Geer, Phys. Rev. D **57** 6989 (1998). S. Geer, FERMILAB-CONF-97-417.
40. Y. Oyama, hep-ex/9803014 (1998).
41. See http://www.hep.anl.gov/NDK/HyperText/minos_tdr.html. P875, "A Long Baseline Neutrino Oscillation Experiment at Fermilab, February, 1995; Dave Ayres for the MINOS collaboration, "Summary of the MINOS proposal, A Long Baseline Neutrino Oscillation Experiment at Fermilab", March 1995; NuMI note: NuMI-L-71, see: http://www.hep.anl.gov/NDK/Hypertext/numi_notes.html
42. See <http://www.aquila.infn.it/icarus/>. C. Rubbia *et al.*, LNGS-94/99 Vol. I & II, (1994). C. Rubbia, Nucl. Phys. Proc. Suppl. **48** 172 (1996).
43. See: <http://www1.na.infn.it/wsubnucl/accel/noe/noe.html>
44. T. Ypsilantis *et al.*, Nucl. Instrum. Meth. **A** 371 330 1996
45. See <http://fn872.fnal.gov/> and <http://fn872.fnal.gov/other/files/UsersMtg98.html>.
46. See: <http://www.neutrino.lanl.gov/BooNE/> E. Chpruch *et al.* FERMILAB-P-0898 (1997).